Geometrical Effects on Non-spherical Extended Systems in Strong Laser Fields

Undergraduate Research Thesis

Presented in Partial Fulfilment of the Requirements for graduation "with Honors Research Distinction in Physics" in the undergraduate colleges of The Ohio State University

by

Pushkar Shirahatti

The Ohio State University

April 2025

Project Advisor: Professor Louis DiMauro, Department of Physics

Geometrical effects on non-spherical extended systems in strong laser fields

Pushkar Shirahatti

The Ohio State University, Department of Physics, Columbus, OH 43210

This work explores how cluster geometry affects ionization in strong laser fields. Using molecular dynamics simulations, spheroidal argon clusters of equal volume but varying aspect ratios were exposed to near-infrared laser pulses (800–2000 nm). Prolate clusters consistently showed higher ion energies and ionization per atom, especially when the laser polarization aligned with the semi-major axis. A peak in energy absorption at 1400 nm suggests a crossover between dipole-enhanced ionization and plasma resonance effects. These results reveal that target geometry and orientation strongly influence laser-cluster interactions, with potential applications in structural probing and laser-driven control of anisotropic systems.

I. INTRODUCTION

With the advent of ultrafast, intense lasers, it has become possible to efficiently convert the energy stored in electromagnetic waves into particle kinetic energy. The physical properties of solids proved them to be efficient targets for energy capture. A new target yet emerged in this field due to its dual-characteristic nature: a density comparable to that of solids and size on the order of individual molecules. Gas-phase clusters (henceforth referred to as clusters) offer insight into both bulk solids and molecules [Castleman, 1988]. Clusters have been shown to be at least as energetic as solids [Ditmire, 1997]. In fact, clusters boast an advantage over both atoms and bulk material with higher energy absorption (per atom) [Batani *et. al.*, 2001]. Strong-field interactions with clusters are particularly interesting because of the plethora of emergent processes, summarized in Fig 1, of which the most pertinent to the subject of this work are energetic electrons and highly charged ions.

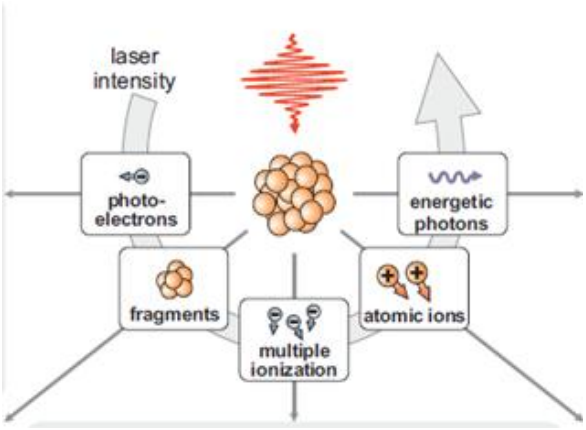

Figure 1: Sourced from Fennel *et. al.*, 2010. A comprehensive list of species which may emerge as a result of intense laser-cluster interactions.

A picture of how a cluster in strong fields disintegrates as shown in Figure 2 is described by three phases of the interacting light pulse [Saalmann *et. al*., 2006]. It was previously believed that in phase I of the pulse, light interacts with the atoms of the cluster individually, i.e. notwithstanding effects of the extended material. Phase II marks the beginning of cluster expansion, due to the creation of ions in the previous phase which repel each other. The ionized electrons remain confined to the bounds of the cluster, while continuing to increase in number due to laser-cluster coupling. As the laser field ionizes a cluster, the released electrons can be field driven back allowing for energetic recollision, giving rise to further ionization and increased ion temperatures [Park *et.al.*, 2022]. In phase III, the energy from the laser diminishes and particle-particle interactions take over. Recombination and thermalization lead to the total disintegration of the cluster. This final phase is also marked by the observables such as energy coming to their resting place.

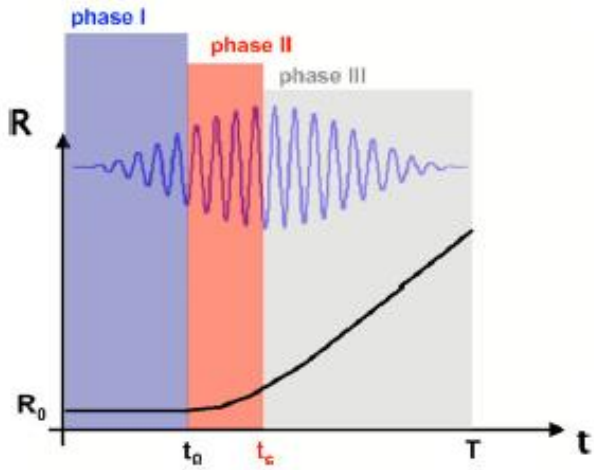

Figure 2: Sourced from Saalmann *et. al.*, 2006. Laser pulse as a function of time shown as blue gaussian sine function. The pulse is broken down into three stages where (broadly speaking) different effects dominate. The cluster radius (R_0) is plotted in black. The cluster size begins to grow during phase II and through phase III.

The microscopic details of ionization, electron heating, and ion expansion are described as follows. Ionization occurs due to a combination of optical field ionization (OFI) and collisional ionization. In OFI, the electric field of the laser temporarily modifies the Coulomb potential of the cluster, making it possible for a bound electron to gain energy and ionize. OFI is important since it is able to produce the conditions necessary (a plasma) early on for further energy absorption [Ditmire *et. al.*, 1996]. Once the system has reached significant ionization per atom due to OFI, inelastic collisions between the free electrons and ions take over to further ionize the system. Collisional ionization has a low intensity threshold for the cluster environment compared to tunnel ionization, so its rate can be quite high [Ditmire *et. al.*, 1996]. Figure 3 (a) shows the two spurts in charge state increase at different points of time in the laser pulse profile for a typical strong-field laser-cluster interaction. The rate of ionization, the solid grey curve, has one peak early in the pulse (this is OFI) and another near the peak of the pulse. In addition to being a mechanism of ionization, electron-ion inelastic collisions also act to heat electrons. Owing to their significantly lower mass compared to parent ions, electrons absorb the majority of the energy deposited into the cluster by the laser. Collisional Inverse Bremsstrahlung (IBS) is a process which occurs whereby an electron gains radiation energy from the laser while scattering in the Coulomb potential of the ions. The rate of this heating mechanism is maximized for a critical electron density. As the density drops due to cluster expansion, the effects from IBS also become less important. The two primary cluster mechanisms are hydrodynamic expansion (HE) and Coulomb explosion (CE). The hot electrons in the cluster have a pressure associated with them, and as they expand they pull the ions out with them [Ditmire *et. al.*, 1996]. The other effect comes from simple Coulombic repulsion that two ions feel in each other's presence. Hydrodynamic pressure goes as $1/r^3$, and Coulomb explosion as $1/r^4$. Thus, CE dominates for small clusters, and HE becomes the dominant process after cluster expansion. As the mean charge state of ions increases, it tends to concentrate on the surface of the cluster. Thus, only the hottest electrons can overcome this effective barrier and become outer ionized.

To model the collective behavior of electrons as they are driven by the laser, Saalmann *et. al.*, 2006 propose a damped, driven model of the center-of-mass of plasma electrons, whose internal frequency Ω matches the laser frequency ω in this equation:

$$\ddot{X}(t) + 2\,\Gamma_t\,\dot{X}(t) + \Omega_t{}^2\,X(t) = F_0(t)\cos\omega t$$

where Γ represents the damping from particle-particle friction, F_0 represents the laser field maximum amplitude, and subscript-t implies that a quantity is time-variant. Picture the ions as one charged shape and the electrons as another shape with the opposite charge. In the rest frame of the ions, the laser shifts the electron cloud in the direction of the laser field, effectively bringing the system out of its equilibrium position. The opposite charges of the two entities acts to enact a restorative force on the electron cloud, while the laser continues to drive the electrons periodically. The motion of the center-of-mass of the electron cloud can thus be solved from the above second-order nonlinear inhomogeneous equation, and the result is $X(t) = A_t\cos(\omega t - \phi_t)$, a sinusoidal motion with a time-dependent amplitude. Figure 3 (c) corroborates these theoretical predictions, as the velocity of the electron cloud is displayed.

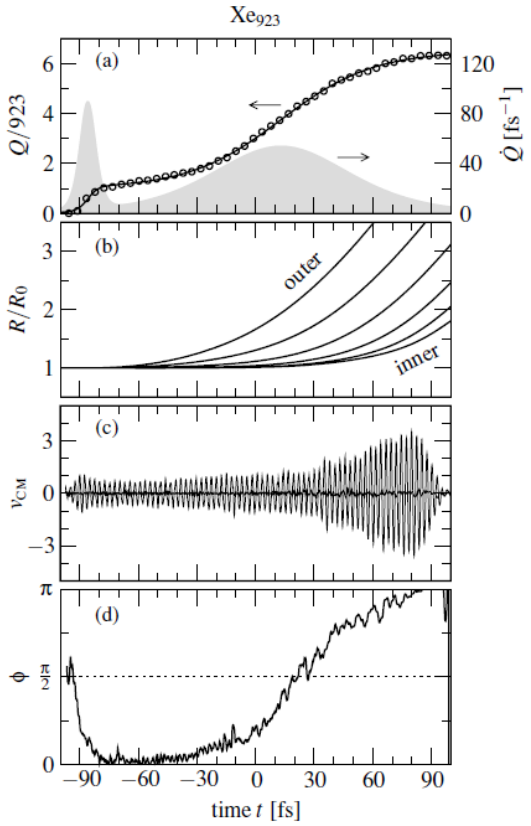

Figure 3: Sourced from Saalmann *et. al.*, 2006. Dynamics of a typical laser-cluster interaction. t = 0 corresponds to the peak of the pulse, with the negative times corresponding to the rising edge and the positive times corresponding to the falling edge. Panel (a) shows the number of ionized electrons in the system normalized to the number of atoms. The solid gray curve shows the time rate of change of this quantity (right hand side axis). Panel (c) shows the velocity of the center of mass of the electrons. Panel (d) shows the phase difference between the driving laser and the motion of the center of mass of electrons.

It was believed for a long time that ionization takes place homogenously and randomly in a cluster. However, experimental observations have shown that under intense laser irradiation, atomic clusters exhibit anisotropic ion yields, with ions preferentially emitted along the laser polarization axis. The anisotropy of ion emission is also shown to be wavelength-dependent—isotropic for shorter wavelengths and increasingly anisotropic at longer wavelengths [Park *et. al.*, 2022]. The anisotropy cannot be explained by HE or CE since these are symmetric processes for spherical clusters. Park *et. al.*, 2022 propose that the laser-induced dipole field is a key contributor as it acts to enhance the electric field at the poles and reducing it in the bulk. Their numerical calculations proved that this enhancement can be as large as 40% at the poles, making them preferential sites for ionization. Though electrons are expected to be released anisotropically due to the dipole effect, the much heavier ions do not acquire their energy from this effect directly. Instead, the inhomogeneous cluster charges expand anisotropically through HE and CE after the pulse ends. The reason for isotropic ion emissions at shorter wavelengths is due to increased IBS heating from electron-ion collisions—whose rate decreases with the wavelength of the laser—which acts to homogenize the charge distribution thereby dominating over anisotropic behavior.

Ion emission anisotropy suggests that ionization in *spherical* extended systems is inherently inhomogeneous, implying that the system's geometry plays a critical role in the interaction process. Despite its significance, this effect remains largely unexplored, with only limited studies. One such work by Grech *et. al.*, 2011 addresses the pure Coulomb explosion of a uniformly charged spheroid cluster. This work shows that the aspect ratio of a spheroid, as defined in Figure 4, has an effect on the dynamics of clusters (sans laser presence). Still it remains an open question—explored in this thesis—how introducing an intense laser to spheroid clusters will affect the system dynamics; interesting effects are expected given that the dipole response from the laser will be geometry dependent. A deeper understanding of this behavior may open new avenues for control and characterization techniques in strong-field and ultrafast physics.

There are many approaches which exist for simulations of laser-clusters interactions. First-principle methods such as density functional theory, though providing a self-contained treatment, are not computationally feasible for clusters of realistic size [Saalmann *et. al.*, 2006]. Molecular dynamics code, on the other hand, is better equipped to model the dynamic cluster environment which sees changes at sub-femtosecond up to nanosecond time scales. This is the approach used in this thesis, and it has been used successfully in the past [Leshchenko *et. al.*, 2023 & Wang *et. al.*, 2020].

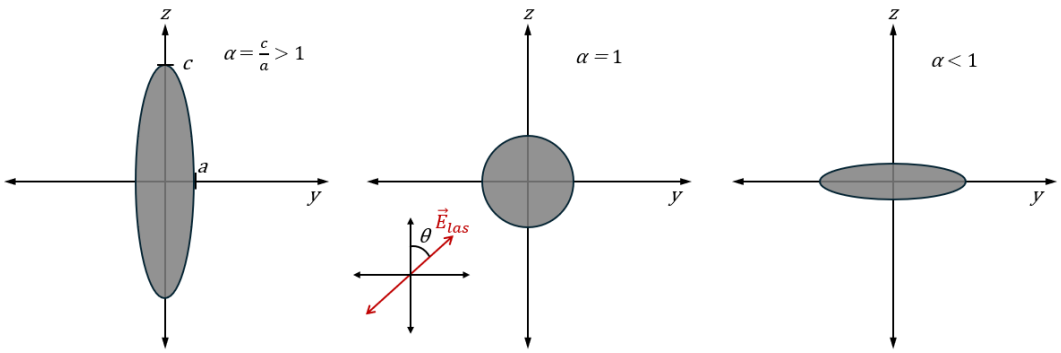

Figure 4: 2D profile of spheroid shapes with different aspect ratios but the same volume. The z-axis is the principal axis when creating the positions of atoms in the cluster, and the form factor α is defined as the ratio between the height in the z-axis to the radius in the xy-axis. The left axes show a *prolate* shape and the right axes show an *oblate* shape. The laser polarization angle θ is made with the yz axis.

The system is constructed by first creating a three-dimensional array of ion positions using spherical icosahedral coordinates. These positions are then scaled to the interatomic distance of Argon (7.1 a.u.). Each ion is individually shifted in a random direction by 0.1 a.u. and the resultant collection of particles is rotated about a random axis in lockstep. To obtain the desired *spheroid* shape from the existing spherical cluster, each ion is evaluated for existing within the bounds of the 3D equation of the shape desired; those existing outside the bounds are "chiseled". Though the various spheroids in this experiment have characteristic aspect ratios, the bounds are chosen such that the same number of particles exist in the final cluster. Ensuring clusters of the same volume are analyzed is crucial to keeping results consistent. An array of electrons is initiated, whereby 1 electron is placed at a random position 0.1 a.u. from each ion. Though Argon has 18 available electrons, the effects on the inner-most 17 are assumed to be shielded from the effects of

the laser or nearby particles. The single active electron approximation has the benefit of reducing the number of active particles in the system. In a scenario where the number of force calculations goes as n^2, this dramatically reduces computational time.

A single pulse of linear polarization is given by the following equation:

$$E = E_0 \cos\left(\frac{2\pi c}{\lambda} t + CEP\right) \cdot e^{\frac{-t^2}{2\sigma^2}}$$

where the FWHM used in the simulation is 90 fs (note that σ, the standard deviation of the gaussian term, is defined by σ ≈ FWHM/2.355). A carrier-envelope phase (CEP) shifts the peak of the cosine function to be on the periphery of the gaussian peak. The angle of laser polarization w.r.t. the system is able to be controlled.

The simulation is started 2 FWHM prior to and terminated 10 ps after peak of the beam, providing ample time for the simulation to capture the laser interaction and consequent molecular dynamics. The particles are propagated using a classical molecular dynamics code. The schema used to propagate in time is the leapfrog method, given by the following Newtonian equations:

$$x_{n+1/2} = x_n + \frac{1}{2} t v_n$$

$$v_{n+1} = v_n + tF\left(x_{n+1/2}\right)$$

$$x_{n+1} = x_{n+1/2} + \frac{1}{2} t v_{n+1}$$

This interleaved update scheme gives rise to the characteristic "leapfrog" pattern in the equations. The position arrays are updated in half steps, with velocity update steps interleaved. The upside of interleaving is that the plasma electron oscillations are properly reproduced; the standard kinematic equations accrue small errors and lead to runaway effects of electron kinetic energy.

Electron-electron and ion-ion force calculations utilize pure Coulomb potential. However, since this potential leads to numerical instability in electron-ion interactions, those are modeled after the soft-core potential,

$$V_{SC} = -\frac{q}{\sqrt{x^2 + y^2 + z^2 + \delta^2}} \quad \ldots (1)$$

which avoids the singularity for electrons sufficiently close to an ion by introducing δ, a quantity dependent on the ionization potential of the ion. The soft-core potential is ineffective for modeling backscattering electrons, so a scattering range is defined, and the scattering motion is enforced on such an electron. Inner ionization occurs when an electron's motion leads its position to exceed the Van der Waals radius of its parent ion, thus creating a quasi-free electron which is not bound to any particular atom but still remains within the cluster. This electron is then propagated classically; some electrons are ejected from the cluster and thus become "outer ionized". An inner-

ionization event leads to the creation of one additional electron in the vicinity of parent ion, and the ion's charge is increased.

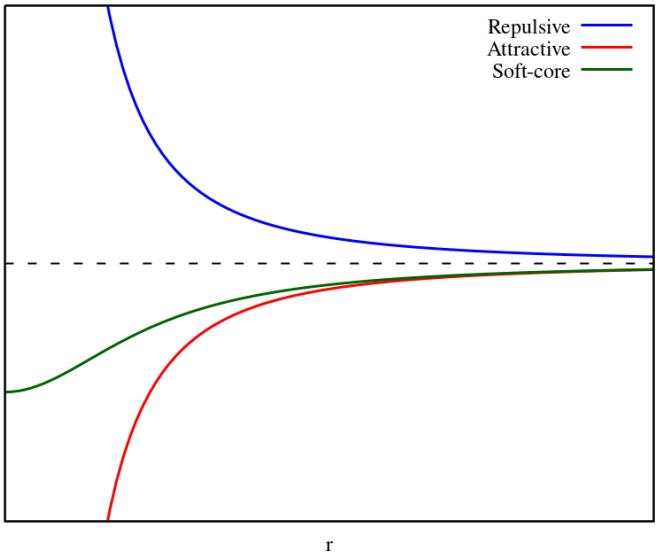

Figure 5: Coulomb repulsive (blue) and attractive (red) potential compared with soft-core attractive potential defined by equation (1). The soft-core models the Coulomb attractive force identically for large r, however at small r it behaves like a potential well whose depth is dependent on the ionization potential of the parent ion.

Figure 5 is illustrative of how, at small distances, the Coulombic attractive acceleration tends to a large value. The simulation code, due to its finite time step, thus overestimates the momentum change of the particle and gives it an unphysical boost; this is a numerical issue. As a result of utilizing the soft-core potential to mitigate this problem, there is a small superfluous acceleration of the ion which must be accounted for. For this reason, ions are frozen in place until the first electron is ionized anywhere in the system. Initially the ions do not repel each other because the system is physically stable.

As the system is exposed to a slight electrical field during the rising edge of the pulse, the electrons and ions organize themselves into tiny dipoles. The system thus has a polarization **P**. The calculation of the strength of the dipole field is described by the equation

$$E_{dip}(\boldsymbol{r}) = \sum_{i}^{N} \frac{1}{\|\boldsymbol{r} - \boldsymbol{r_i}\|^3} [3(\hat{\boldsymbol{n}} \cdot \hat{\boldsymbol{r}})\hat{\boldsymbol{r}} - \hat{\boldsymbol{n}}] \qquad \ldots (2)$$

Where $\boldsymbol{n}$ signifies the laser polarization direction, and $i \ldots N$ signify the ions of the system [Jackson, 1999]. The dipole field is only calculated at the surface of the spheroid.

II. RESULTS

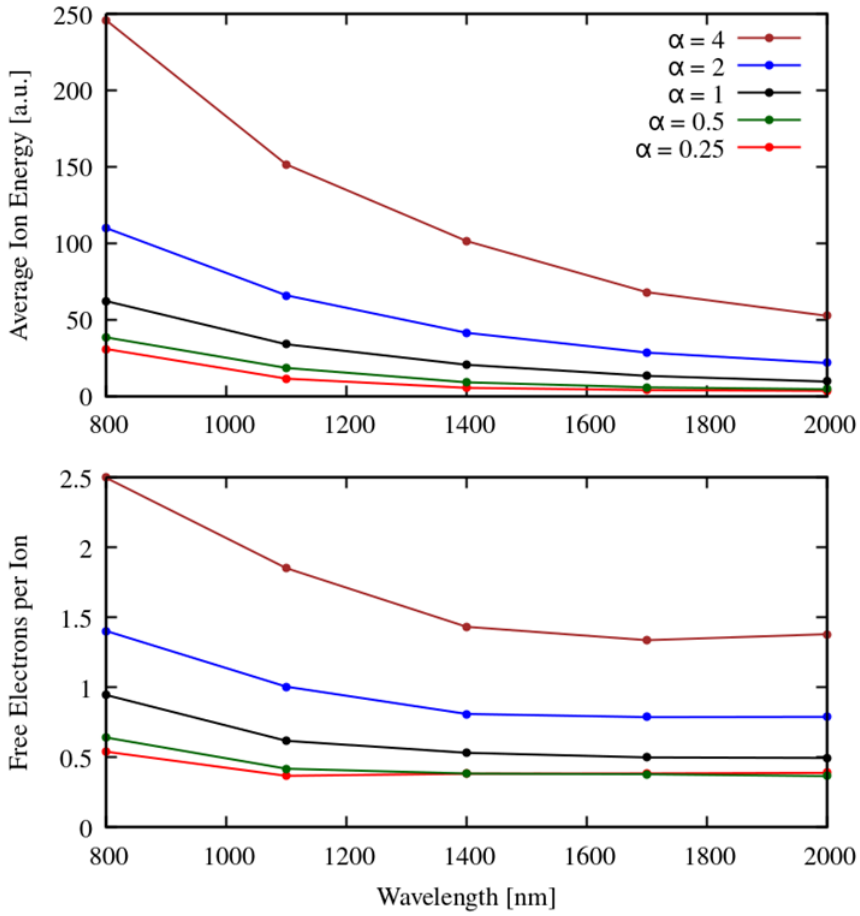

Figure 6: (Top) Average ion energy of clusters of 5 aspect ratios (laser parameters I = 300 TW/cm^2 and τ = 90 fs) varied by wavelength. (Bottom) Free electrons in system divided by number of ions in cluster.

Five spheroidal target geometries were investigated, ranging from highly prolate (aspect ratio α = 4) to highly oblate (α = 0.25). The average ion energy and ionization per ion were evaluated 1 picosecond after the peak of the laser pulse, and the results are shown in Figure 6. My findings show that across the near-infrared (NIR) wavelength range of 0.8–2 μm, prolate targets consistently exhibited higher ion energetics and greater ionization per ion compared to oblate shapes. This trend highlights the critical role of target geometry in energy absorption and plasma formation. The system energetics prominently increase for shorter wavelengths, indicating that resonant plasma absorption becomes a dominant energy absorption mechanism, as the system is driven closer to resonance—approximately 200 nm for this system. Prolate targets show a substantial ionization response to driving wavelength, while oblate targets remain largely unaffected, suggesting that the driving laser frequency is highly detuned to the modified potential well of an oblate cluster. Ionization appears to converge to a value. Some shapes (prolate) are robust and some (oblate) resistant to ionization compared to their spherical counterparts.

To further probe the geometry-dependent response, simulations were performed for the most extreme shapes (prolate $\alpha = 4$ and oblate $\alpha = 0.25$) under laser pulses of 0.8 μm and 2 μm, while varying the polarization angle with respect to the target's principal axis. Figure 7 illustrates that for both wavelengths, prolate shapes exhibit superior ion energy and ionization up to a polarization angle of 60°. At this angle, the behavior of the two shapes becomes comparable, and beyond this angle the oblate shape dominates the prolate in energy absorption. It is apparent that energy absorption and ionization is maximized as the polarization angle runs parallel to the semi-major axis of the target shape. However, there is an asymmetry as the laser polarization angle aligns with the semi-minor axis of the oblate cluster: this geometry does not fully restore to the absorption seen in the prolate cluster with the laser parallel to its semi-major axis. This hints at the role of geometric effects in enhancing energy absorption.

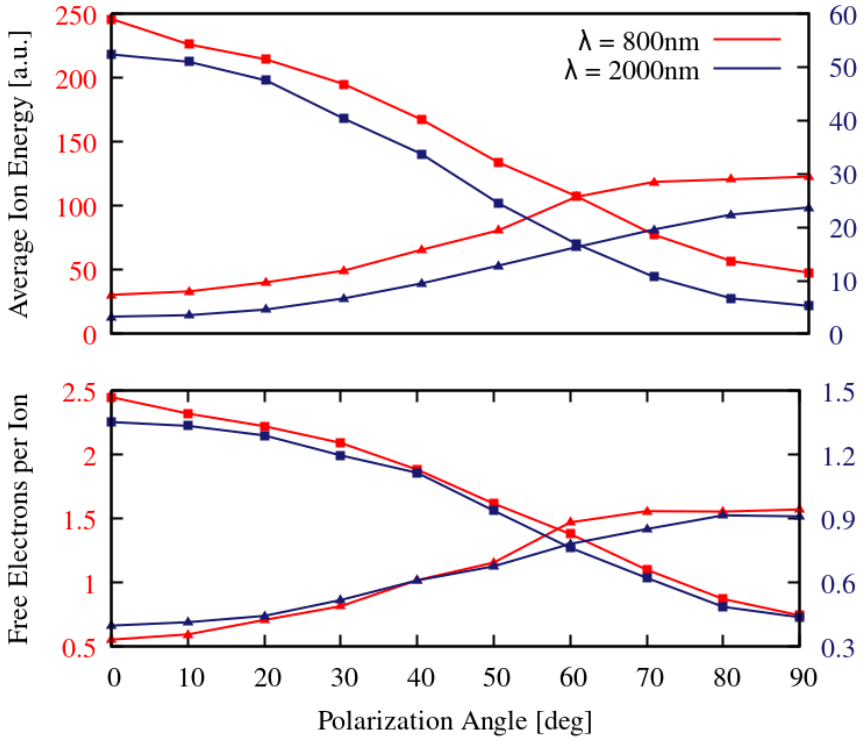

Figure 7: Average ion energy of oblate $\alpha = 0.25$ (triangle) and prolate $\alpha = 4$ (square) clusters with the polarization angle of laser with respect to principal axis. Note the left y-axis is for the 800 nm plots (red) and the right y-axis is for the 2000 nm plots (blue).

While the discussion so far has been centered on the dynamics of the system as a whole—focusing on observables such as the average ionic charge or energy—additional information can be obtained by taking a careful look at the ion energy distribution. The results shown in Figure 8 are in agreement with previously reported data for comparable systems. All spectra display the "knee-shape" characteristic of clusters under strong-field irradiation. At an 800 nm wavelength laser, the prolate system has maximum ion yield of 22 keV, which is enhanced compared to the cutoff of 8 keV and 5 keV for spherical and oblate clusters, respectively. The spectra exhibit the presence of two processes: in the low-energy region there is a linear relationship which transitions into a flat distribution for the high-energy region. Figure 8 is plotted on a logscale, so the linear

fit actually corresponds to an exponential decay in this region, which suggests that ions in this energy range are in thermal equilibrium (thus following a Maxwell distribution). The flat region of the distribution is indicative of ions undergoing Coulomb explosion. Interestingly, looking at the top panel, the prolate cluster appears to be far from thermal equilibrium due to the broad, flat spectrum whereas the spherical and oblate clusters clearly display a linear distribution. Thus the cluster geometry has an effect on the interplay between HE and CE, two processes in ion dynamics.

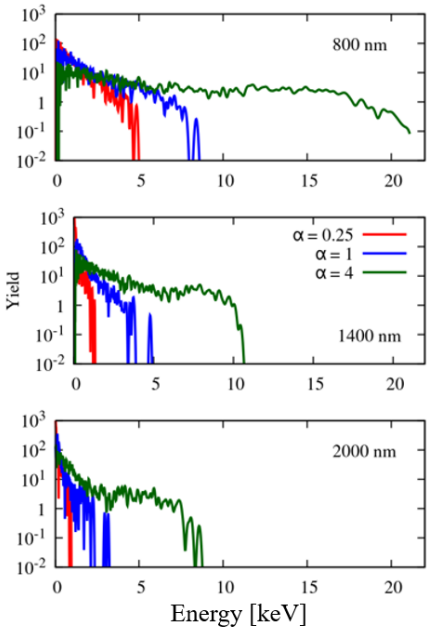

Figure 8: Ion energy spectra on y-logscale for 800 nm (top), 1400 nm (middle), and 2000 nm (bottom) at the end of molecular dynamics simulation (1 ps after peak). Red plots are oblate $\alpha = 0.25$, blue plots are sphere, and green plots are prolate $\alpha = 4$.

Furthermore, Figure 8 is also evidence that changing wavelength of the laser has an effect on the ratio of mean ion energy between prolate and oblate shapes; though it is expected that in general all clusters absorb less energy for higher wavelengths, it is interesting that this ratio does not remain fixed. Figure 9 shows the ratio of mean ion energies between the prolate ($\alpha = 4$) and oblate ($\alpha = 0.25$) for different wavelengths. The ion energy ratio ranges from 8-fold to 20-fold, and peaks in the middle of the NIR range at 1400 nm. Another ratio is introduced on the right panel (which scales the difference in energy between shapes to the combined energy of both shapes). This also shows a prominent peak at 1400 nm. Below approximately 1100 nm, the increasing influence of plasma effects begins to counteract the dipole-enhanced ionization mechanisms associated with geometric asymmetry. This is supported by features in the energy spectrogram, suggesting a crossover regime where plasma and dipole contributions are equally significant.

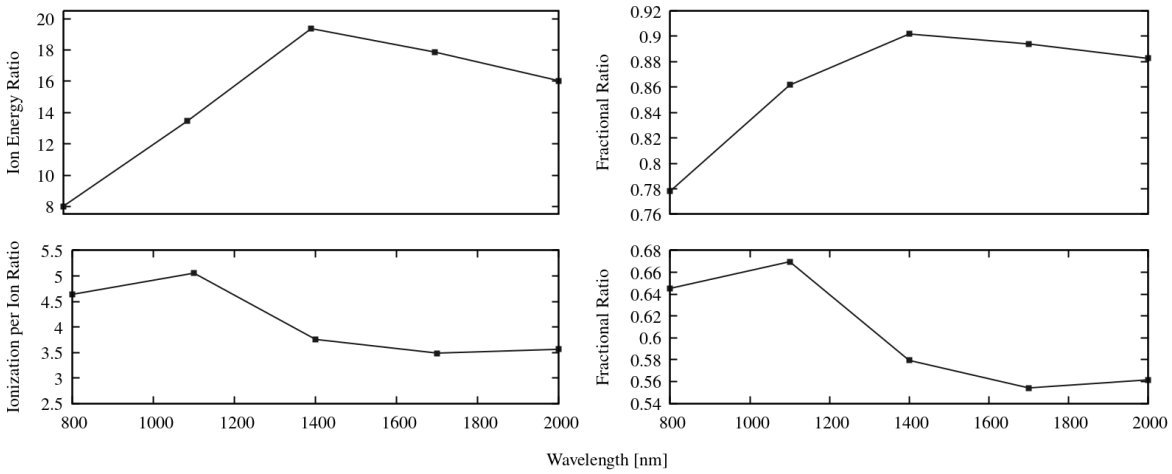

Figure 9: Left panels show the ratio between prolate α = 4 and oblate α = 0.25 mean ion energy $\langle E_{Prol.}\rangle / \langle E_{Obl.}\rangle$ at the end of the simulation across wavelengths. Right panels show the calculation of a fractional ratio: $\langle E_P\rangle - \langle E_O\rangle / \langle E_P\rangle + \langle E_O\rangle$. The same calculations are repeated for the ionization per ion in the bottom panels.

The state of the ions at the time of the peak of the pulse is visualized in Figure 10. The prolate shape appears to be further disintegrated than the spherical or oblate clusters. The oblate cluster shows how the core ions are at a lower charge state (retaining more electrons per ion) in the core of the cluster while the surface ions are ionized to +7 charge states. Though the discrepancy is not as pronounced, the same is seen in the spherical and prolate clusters. Most of the ions have ionized to charge states of +10 or above, which explains the disintegration due to Coulomb repulsion. The higher charge states along the surface make clear the effect of the dipole response in clusters.

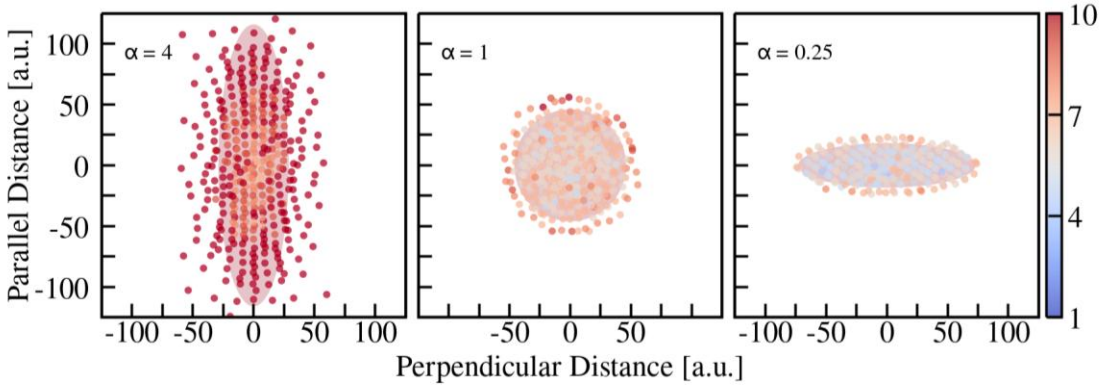

Figure 10: Ion positions at the peak of the pulse (180 fs from simulation start). The shape of the cluster before exposure to pulse is shown in light-red beneath the ions (left: prolate, middle: sphere, right: oblate). The color box on the right represents ionic charge states ranging from +1 to +10. Ions with +15 charges are observed, though these are assigned this maximum value.

Similar visualizations for clusters angled at lasers with polarization angles of 30º, 60º, and 90º are shown in Figure 11. As the laser is angled further away from the semi-major axis of the prolate chape, the cluster absorbs less energy since the charge state drops dramatically and the cluster does not disintegrate much from its original geometry; it is still in the quasi-neutral state, where electrons are mainly inner ionized. Conversely, as the laser is angled towards the semi-major axis of the oblate shape, higher charged ions and greater ion dynamics are observed as the ions closest to the surface become charged to +10. In agreement with the observations from Figure 2, the oblate shape with the laser aligned to its semi-major axis is still not as energetic as the prolate shape seen in Figure 11. The geometric differences which arise from the spherical symmetry about the z-axis of spheroids shows that describing the dipole response is complicated, despite the shapes having the same ratio between semi-major and semi-minor axes.

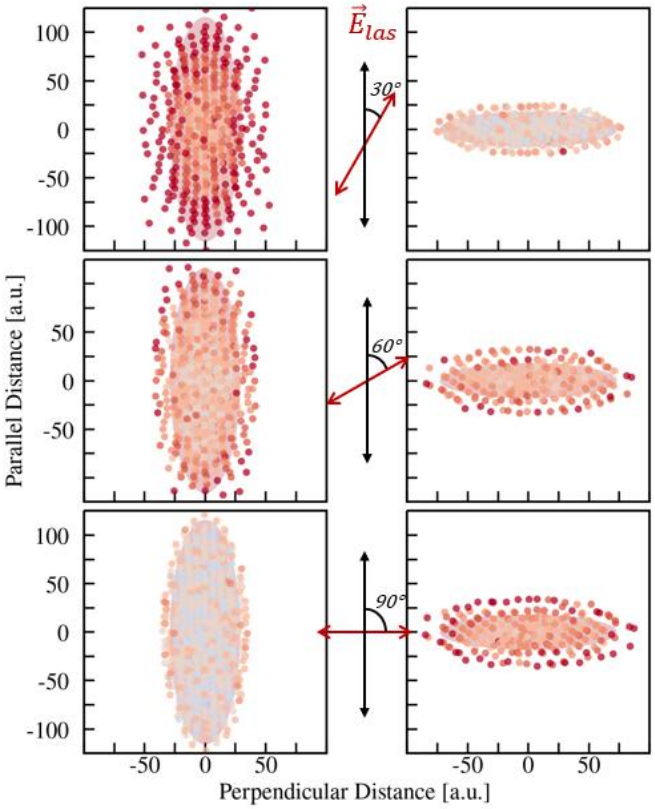

Figure 11: Visualizations of the ions at the peak of the pulse (180 fs from simulation start) for the prolate α=4 shape (left panels) and oblate α=0.25 shape (right panels) for various laser polarization angles as marked.

To investigate how much of an effect the dipole field is having on energy absorption in spheroid cluster, a numerical calculation was done at 1 interatomic distance away from the surface of the cluster (Figure 12). At the poles, the induced dipole field is parallel to the laser polarization, thereby enhancing ionization in this region. At the equator, the induced dipole field is anti-parallel, thereby diminishing the total electric field experienced by the cluster in this region. The dipole field for various shapes is quantified in Figure 13. The poles experience a higher response than

the equators for shapes more prolate than the α=0.25 shape. Interestingly, the field enhancement at the poles peaks at α=2, so the intuition that more prolate shapes necessarily lead to an increased dipole response is incorrect.

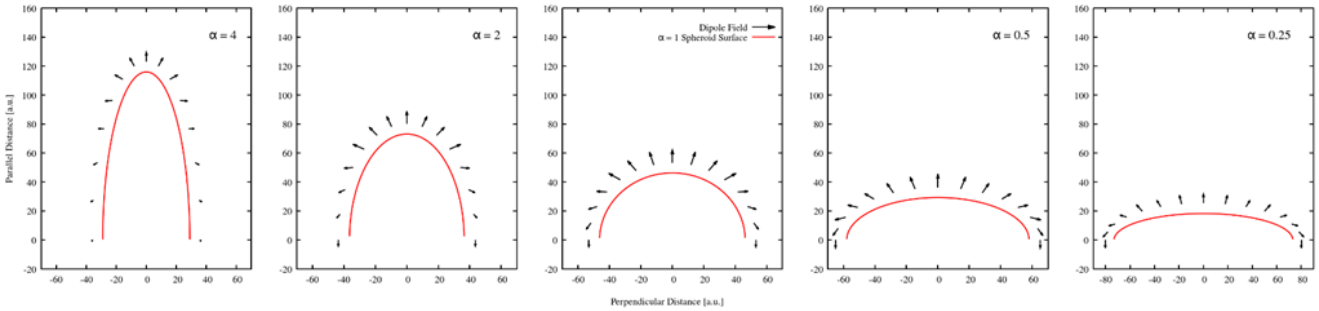

Figure 12: Dipole field (black) calculated qualitatively using equation (2) at 1 interatomic distance (7.1 a.u.) away from the surface of the cluster (red). Laser polarization direction is up-down.

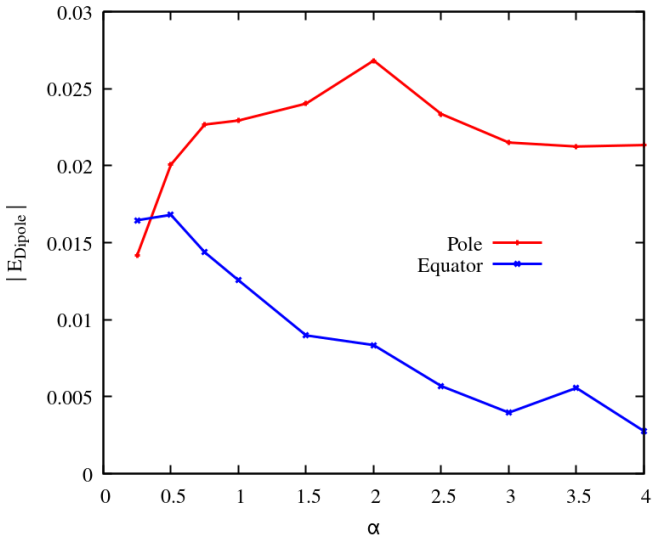

Figure 13: Dipole field response (as seen in Figure 12) magnitude at two positions: the pole (red) and equator (blue), plotted as a function of aspect ratio.

III. DISCUSSION & CONCLUSION

This work demonstrates the interplay between geometry, wavelength, and polarization in energy absorption in laser-irradiated clusters. After extensive investigation of varying the shape of the clusters, it was shown that prolate clusters outperform their spherical and oblate counterparts in ion energetics and ionization per atom under the same light pulse parameters. Additionally, it was observed that orienting a spheroid cluster's semi-major axis along the laser polarization maximizes this effect.

Calculations of the prolate-to-oblate ratio of mean system energy after 1 ps propagation revealed a significant result of a peak occurring at 1400 nm; despite being in a wavelength regime

that is usually considered far detuned from the plasma frequency, longer-wavelength pulses did not exhibit a unidirectional trend. This behavior can be explained by the existence of two separate effects acting as counteracting pressures on the ion energetics. As has been proposed by Park, et. al., 2022 , dipole effects are effective on clusters shined with pulses of upwards of 2000 nm. Whereas for pulses of shorter wavelengths, plasma frequency effect become increasingly important. In Figure 14, I propose a mechanism by which the geometry of the clusters may explain increased energy attenuation for shorter wavelengths. Due to the symmetry of spherical shapes, the potential well corresponding to the cluster remains the same in all directions. Meanwhile for spheroid shapes the potential well's width, being proportional to the amount of material extending in that direction, is wider in the direction of the semi-major axis and narrower in the direction of the semi-minor axis. Thus there are effectively two basis resonant frequencies for each axis. For the two clusters considered in Figure 14 (a), one being prolate and one oblate, the effective plasma frequency is higher for the prolate case. This shift of the prolate cluster's plasma frequency brings it closer to the laser frequency, and this appears as enhanced energy absorption. The two wavelength-dependent effects—dipole response and plasma resonance—arrive at a crossover point at 1400 nm where both geometric effects contribute to enhance energy absorption in the prolate shape preferably to the oblate shape.

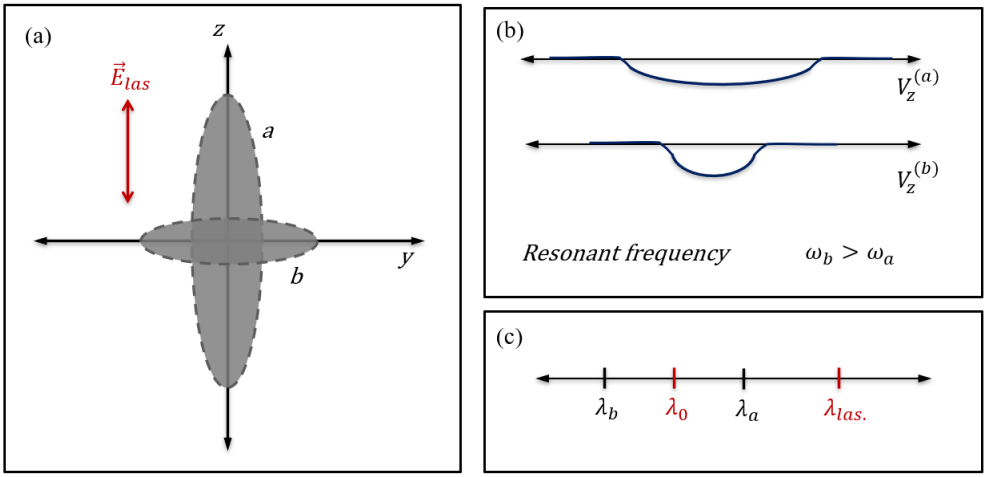

Figure 14: (a) a prolate shape and oblate shape. (b) widening and narrowing of potential created by the plasma leading to differential plasmonic frequency. (c) due to the differential potential wells of the shapes, shape *a* becomes more in-tune with the laser wavelength as shape *b* shifts away. λ_0 corresponds to the resonant laser wavelength for a spherical cluster, while λ_a corresponds to the prolate shape.

Despite this peak at 1400 nm, the ratio between the prolate and oblate clusters' mean ion energy does not drop below 8 in the wavelengths investigated (800 – 2000 nm). Therefore lasers of this wavelength are a good candidate to detect the presence of prolate shapes in a sample, since the (at least) eightfold energy range on the ion spectra comes exclusively from them. Additionally, this method may act as a method to time a process which involves a spheroid target changing shape.

Charge state visualizations at the peak of the pulse shed further light on these interpretations. The higher charge states concentrated near the surface of prolate clusters reveal

strong surface field enhancements while oblate clusters remain quasi-neutral at the midpoint of time profile of the pulse. This work only focused on comparing the most prolate and most oblate shapes to a spherical cluster, so further analysis for intermediate shapes is necessary to describe the collective behavior of charged ions in the system. Additionally, wavelength-dependent effects on the charge state of ions should also be investigated to ascertain if dipole, plasma resonance, or both effects contribute.

In addition to the geometry, the polarization angle with respect to target cluster has a noticeable effect for spheroid clusters. The drop-off in system energetics and ionization as the polarization angle moves away from the semi-major axis warrants further research on the topic. Studying orientation effects in larger systems would allow for experimental setups that are able to resolve and/or select the orientation of important targets such as biomolecules. Additional future work includes confirming the asymmetry of a spheroid cluster does lead to a differential in the plasmonic response along different axes. Observing an increase in magnitude of the dipole field enhancement for more prolate shapes until $\alpha = 2$, and a subsequent drop, was unexpected. Perhaps further analytical treatment could explain the complexity observed.

IV. ACKNOWLEDGEMENTS

The simulations contained in this thesis were made possible with the College of Arts & Sciences' Unity Cluster. I would also like to recognize Prof. Louis DiMauro. My participation in his lab group was formative to my undergraduate experience. A special thanks to Dr. Abraham Camacho-Garibay for sharing his molecular dynamics code and being a supportive mentor.

WORKS CITED

U. Saalmann, C. Siedschlag, and J. M. Rost, "Mechanisms of cluster ionization in strong laser pulses," J. Phys. B 39(4), R**39**—R77 (2006). https://doi.org/10.1088/0953-4075/39/4/r01

T. Fennel, K. H. Meiwes-Broer, J. Tiggesbäumker, P. G. Reinhard, P. M. Dinh, and E. Suraud, "Laser-driven nonlinear cluster dynamics," Rev. Mod. Phys. **82**(2), 1793–1842 (2010). https://doi.org/10.1103/revmodphys.82.1793

T. Ditmire, T. Donnelly, A. M. Rubenchik, R. W. Falcone, and M. D. Perry, "Interaction of intense laser pulses with atomic clusters," Phys. Rev. A **53**(5), 3379–3402 (1996). https://doi.org/10.1103/physreva.53.3379

M. Grech, R. Nuter, A. Mikaberidze, P. Di Cintio, L. Gremillet, E. Lefebvre, U. Saalmann, J. M. Rost, and S. Skupin, "Coulomb explosion of uniformly charged spheroids," Phys. Rev. E **84**(5) (2011). https://doi.org/10.1103/physreve.84.056404

Z. Wang, A. Camacho Garibay, H. Park, U. Saalmann, P. Agostini, J. M. Rost, and L. F. DiMauro, "Universal High-Energy Photoelectron Emission from Nanoclusters Beyond the Atomic Limit," Phys. Rev. Lett. **124**(17) (2020). https://doi.org/10.1103/physrevlett.124.173201

H. Park, A. Camacho Garibay, Z. Wang, T. Gorman, P. Agostini, and L. F. DiMauro, "Unveiling the Inhomogeneous Nature of Strong Field Ionization in Extended Systems," Phys. Rev. Lett. **129**(20) (2022). https://doi.org/10.1103/physrevlett.129.203202

V. Leshchenko, B. Smith, A. Camacho Garibay, P. Agostini, L. F. DiMauro, and L. Fang, "Nanoplasma resonance condition in the middle-infrared spectral range," Phys. Rev. E **107**(5) (2023). https://doi.org/10.1103/physreve.107.055207

T. Ditmire, R. A. Smith, J. W. G. Tisch, and M. H. R. Hutchinson, "High Intensity Laser Absorption by Gases of Atomic Clusters," Phys. Rev. Lett. **78**(16), 3121–3124 (1997). https://doi.org/10.1103/physrevlett.78.3121

Batani, D., C. J. Joachain, S. Martellucci, and A. N. Chester, 2001, Eds., *Atoms, Solids, and plasmas in Super-Intense Laser Fields* (Kluwer, New York).

A. W. Castleman and R. G. Keesee, "Gas-Phase Clusters: Spanning the States of Matter," Science **241**(4861), 36–42 (1988). https://doi.org/10.1126/science.241.4861.36

J. D. Jackson, *Classical electrodynamics*, 3rd ed. (Wiley, New York, 1999).